AIAA JOURNAL
Vol. 56, No. 2, February 2018

Flow Features near Plate Impinged by Ideally Expanded and Underexpanded Round Jets

Romain Gojon*
KTH Royal Institute of Technology, 114 28 Stockholm, Sweden
and
Christophe Bogey†
Central School of Lyon, 69134 Ecully Cedex, France

DOI: 10.2514/1.J056421

The properties of the flow near the plate and in the wall jets have been investigated from large-eddy simulation data of round impinging jets. Four jets are underexpanded and four jets are ideally expanded, which allowed examination of the influence of the presence of shock-cell structures. The underexpanded jets are characterized by a fully expanded Mach number of 1.56 and an exit Mach number of 1. The ideally expanded jets have a Mach number of 1.5. The Reynolds number of the eight jets is equal to 6×10^4. The jets impinge normally on a flat plate located from $4.16r_0$ to $12r_0$ downstream of the nozzle and generate acoustic tones due to an aeroacoustic feedback mechanism. In this paper, the near pressure and density fields of the jets are characterized using Fourier transform on the nozzle exit plane, the plate, and an azimuthal plane. First, mean and rms radial velocities of the wall jets are examined. The impact of the shock-cell structure on the wall jet is discussed. The pressure spectra on the plate are then shown as a function of the radial coordinate. The tone frequencies are all visible where the jet shear layers impinge the plate, but only some of them emerge in the wall jet created after the impact. For the ideally expanded jets, the temporal organization of the wall jet along the frequencies of the feedback mechanism decreases with the nozzle-to-plate distance, but for the nonideally expanded jets, this organization is linked to the oscillation of the Mach disk located just upstream of the plate. Consecutively, the amplitude and the phase fields at the tone frequencies are represented on the three planes mentioned earlier. Similar spatial organizations of the turbulent structures are found in the jet shear layers and in the wall jets. Thus, axisymmetric and helical arrangements of the structures in the jet shear layers lead to concentric and spiral distributions of the structures on the plate, respectively. In particular, for one of the underexpanded jets, a spiral shape and concentric rings, associated with two tone frequencies generated simultaneously, are observed on the flat plate in the pressure and density phase fields. Finally, the convection velocity of the turbulent structures at the tone frequencies in the wall jets are evaluated based on phase fields, and the mean convection velocity is computed using cross correlations of radial velocity. The results are in good agreement with those from a recent experimental study of ideally expanded impinging jets.

Nomenclature

a_e	=	speed of sound at nozzle exit, m/s
a_j	=	speed of sound in ideally expanded equivalent jet, m/s
D	=	diameter of jet, m
D_j	=	diameter of ideally expanded equivalent jet, m
f	=	frequency, Hz
L	=	nozzle-to-plate distance, m
M_e	=	exit Mach number, equal to u_e/a_e
$\mathcal{M}_j$	=	Mach number of ideally expanded equivalent jet
u_c	=	convection velocity, m/s
u_e	=	velocity at nozzle exit, m/s
u_j	=	velocity of ideally expanded equivalent jet, m/s
r_0	=	radius of jet, m
St	=	Strouhal number, equal to fD_j/u_j

I. Introduction

HIGH-SUBSONIC and supersonic jets impinging on a flat plate have been studied by many researchers during the past decades, notably by Powell [1] and Wagner [2]. Very intense tones have been observed in the acoustic field. Powell [1] suggested that such tones are generated by an aeroacoustic feedback mechanism involving the turbulent structures propagating downstream from the nozzle to the plate and the acoustic waves propagating upstream from the plate to the nozzle.

For subsonic impinging round jets, the tone frequencies are well predicted by the model proposed by Ho and Nosseir [3] and Nosseir and Ho [4]. Round supersonic jets impinging on a flat plate normally have been investigated experimentally by Henderson and Powell [5], Krothapalli et al. [6], and Henderson et al. [7], among others. In some cases, a feedback mechanism is observed, as in subsonic jets. This is very often the case when the jet is ideally expanded, but this happens only for some nozzle-to-plate distances when the jet is imperfectly expanded. In the latter case, Henderson and Powell [5] suggested that the feedback loop establishes only when a Mach disk forms just upstream from the plate. More recently, for underexpanded impinging jets, Risborg and Soria [8] explored the instability modes of the jets using ultra-high-speed schlieren and shadowgraph techniques. Notably, axial and helical modes were visualized, and the Mach disk located just upstream from the plate was found to oscillate. For similar jets, Buchmann et al. [9] pointed out the periodic formation of large-scale structures in the jet shear layers using a high spatial resolution schlieren imaging. The complete feedback mechanism, including large-scale structures in the shear layers propagating downstream from the nozzle to the plate and acoustic waves propagating upstream from the plate to the nozzle, was visible. Mitchell et al. [10] studied the periodic oscillations of the shear layer of underexpanded impinging jets using time-resolved schlieren image sequences.

Presented as Paper 2016-2929 at the 22nd AIAA/CEAS Aeroacoustics Conference, Lyon, France, 30 May–1 June 2016; received 12 June 2017; revision received 31 August 2017; accepted for publication 4 September 2017; published online 6 October 2017.

*Postdoctoral, Department of Mechanics, Linné FLOW Centre; gojon@kth.se. Member AIAA.

†Research Scientist, Laboratoire de Mécanique des Fluides et d'Acoustique, UMR CNRS 5509, Université de Lyon; christophe.bogey@ec-lyon.fr. Senior Member AIAA.

For underexpanded impinging jets, the presence of recirculation zones near the plate and the dynamic of the fluid between the Mach disk created just upstream of the plate and the plate was investigated experimentally by Henderson et al. [7]. Notably, tones were found to be produced in the peripheral supersonic flow. Recirculation zones were also observed between the near-wall Mach disk and the flat plate for some nozzle-to-plate distances by Krothapalli et al. [6]. Kuo and Dowling [11] derived a model considering pressure waves and entropy fluctuations to explain the oscillation modes of the jet at the feedback tone frequencies. Numerically, Dauptain et al. [12,13] proposed a new path for the aeroacoustic feedback mechanism passing through the wall jet created after the jet impact. More recently, Weightman et al. [14] analyzed the dynamic of the creation of an acoustic wave at the plate surface using ultra-high-speed schlieren. Finally, Davis et al. [15] studied the wall pressure oscillations in ideally expanded impinging jets using a fast-response pressure-sensitive paint on the plate. They identified axisymmetrical and helical oscillation modes of the jets associated with tone frequencies thanks to phase-conditioned schlieren images. For such modes, they presented the phase-averaged distributions of the fluctuating pressure on the flat plate. The turbulent structures organized axisymmetrically or helically in the jet shear layers were shown to persist after the impact, as they propagate radially in the wall jets, even several diameters away from the jet axis. The turbulent organization in the wall jet created after the impact is thus of primary interest to gain insights on the flow and acoustic properties of supersonic impinging jets. However, it has rarely been described in the past, notably because of experimental difficulties to perform measurements in this region with particle image velocimetry techniques due to the reflections coming from the plate. This is fortunately not the case using recent fast-response pressure-sensitive paint. Indeed, Davis et al. [15] can reach a frequency resolution of several kilohertz, permitting study of mechanisms like the feedback loop establishing in supersonic impinging jets.

In previous studies by the authors [16,17], the feedback loop and the associated oscillations of the jets have been studied. In this paper, the azimuthal organization of turbulent structures in the jet shear layers and on the flat plate, in the wall jets created after the impact, are characterized from data provided by large-eddy simulations. The aerodynamic and acoustic properties of the eight jets have been detailed previously in Gojon and Bogey [16] for the nonideally expanded jets and in Bogey and Gojon [17] for the ideally expanded jets. The spatial organization and the convection velocity of the turbulent structures in the wall jet are examined from the pressure and density fields on the plate. The effects of the presence of shock-cell structures are sought. The paper is organized as follows. The jet conditions and the numerical parameters are presented in Sec. II. Snapshots of two jets and the properties of the aeroacoustic feedback loop establishing in the jets are provided in Sec. III. In Sec. IV, the mean and rms fields of the radial velocity in the wall jets are shown. An analysis of the turbulent structures in the jet shear layers and in the wall jets is also conducted by plotting the amplitude and phase fields of the pressure and density fields at the tone frequencies. Concluding remarks are finally given in Sec. V.

II. Parameters

A. Jet Conditions

In this section, the main jet conditions are provided. More information can be found in previous papers [16,17]. The jets have a temperature ratio (TR) $\mathrm{TR} = T_r/T_{\mathrm{amb}} = 1$, where T_r and T_{amb} are the stagnation and the ambient temperatures. They originate from a pipe nozzle of radius r_0, for which the lip is $0.1r_0$ thick. At the nozzle inlet, a Blasius mean velocity profile is imposed with a boundary-layer thickness of $0.15r_0$.

For the ideally expanded jets, the nozzle-to-plate distances L are respectively equal to $6r_0$, $8r_0$, $10r_0$, and $12r_0$, as shown in Table 1. The jets are thus referred to as JetidealL6, JetidealL8, JetidealL10, and JetidealL12. They have an exit Mach number of $\mathcal{M}_e = u_e/a_e = 1.5$, where u_e and a_e are the exit velocity and the speed of sound in the jet, and a Reynolds number of $Re_j = u_e D/\nu = 6 \times 10^4$, where $D = 2r_0$ is the nozzle diameter and ν is the kinematic molecular viscosity. The jet ejection conditions and the nozzle-to-plate distances are identical to those in the experimental study of Krothapalli et al. [6], whereas the jet Reynolds number is one order of magnitude lower than the experimental one.

Table 1 Mesh parameters

	L[a]	n_r[b]	n_θ	n_z	Total no. of points
JetidealL6	$6r_0$	500	512	791	202×10^6
JetidealL8	$8r_0$	500	512	803	205×10^6
JetidealL10	$10r_0$	500	512	869	222×10^6
JetidealL12	$12r_0$	500	512	936	240×10^6
JetunderL4	$4.16r_0$	500	512	668	171×10^6
JetunderL5	$5.6r_0$	500	512	764	195×10^6
JetunderL7	$7.3r_0$	500	512	780	200×10^6
JetunderL9	$9.32r_0$	500	512	847	217×10^6

[a]L is the nozzle-to-plate distance.
[b]Number of points n_r, n_θ, and n_z in the radial, azimuthal, and axial directions, respectively.

For the nonideally expanded jets, the nozzle-to-plate distances L are equal to $4.16r_0$, $5.6r_0$, $7.3r_0$, and $9.32r_0$ (see also in Table 1). The jets are thus denoted as JetunderL4, JetunderL5, JetunderL7, and JetunderL9. They have an ideally expanded Mach number of $\mathcal{M}_j = u_j/a_j = 1.56$, where u_j and a_j are the exit velocity and the speed of sound in the ideally expanded equivalent jet. Their Reynolds number is $Re_j = u_j D_j/\nu = 6 \times 10^4$, where D_j is the nozzle diameter of the ideally expanded equivalent jet. The exit Mach number is $\mathcal{M}_e = 1$. The ejection conditions of the jets and the nozzle-to-plate distances are identical to those in the experiments of Henderson et al. [7], and the jet Reynolds number is one order of magnitude lower than the experimental one.

B. Numerical Parameters

In the large-eddy simulation (LES), the unsteady compressible Navier–Stokes equations are solved on cylindrical meshes (r, θ, z) using an explicit six-stage Runge–Kutta algorithm for time integration and low-dissipation and low-dispersion explicit 11-point finite differences for spatial derivation [18,19]. At the end of each time step, a high-order filtering is applied to the flow variables to remove grid-to-grid oscillations and to dissipate subgrid-scale turbulent energy [20–22]. The radiation conditions of Tam and Dong [23] are implemented at the boundaries of the computational domain, in combination with a sponge zone at the outflow boundaries, combining grid stretching and Laplacian filtering to damp turbulent fluctuations and acoustic waves before they reach the boundaries. Adiabatic no-slip conditions are imposed at the nozzle walls and at the flat plate. Finally, a shock-capturing filtering is applied to avoid Gibbs oscillations near shocks [24]. The axis singularity is treated with the method proposed by Mohseni and Colonius [25]. A reduction of the effective resolution near the origin of the polar coordinates is also implemented [26]. Finally, a forcing [27] is added in the boundary layer in the nozzle to generate velocity fluctuations at the nozzle exit. This procedure enables one to reach peak turbulent intensities between 2.6% for JetidealL12 and 7.3% for JetunderL4.

The simulations are carried out using an OpenMP-based in-house solver, and a total of 250,000 or more iterations are performed in each case after the transient period. The simulation time is equal to $1250r_0/u_j$ or more. The cylindrical meshes contain between 171 and 240 million points, as reported in Table 1. The minimal axial mesh spacing, equal to $\Delta z = 0.0075r_0$, is located near the nozzle lip and the flat plate, and the maximal axial mesh spacing, equal to $\Delta z = 0.03r_0$, is located between the nozzle and the plate. The minimal radial spacing is equal to $\Delta r = 0.0075r_0$ at $r = D/2$, and the maximal radial spacing, excluding the sponge zone, is $\Delta r = 0.06r_0$ for $5r_0 \le r \le 15r_0$. The maximum mesh spacing of $0.06r_0$ allows acoustic waves with Strouhal numbers up to $St = fD_j/u_j = 5.3$ to be well propagated in the computational domains, where f is the frequency. Thus, the computational domain, excluding the sponge zones, extends from $6r_0$ upstream of the nozzle exit to the plate in the axial direction and from $-15r_0$ to $15r_0$ in the radial

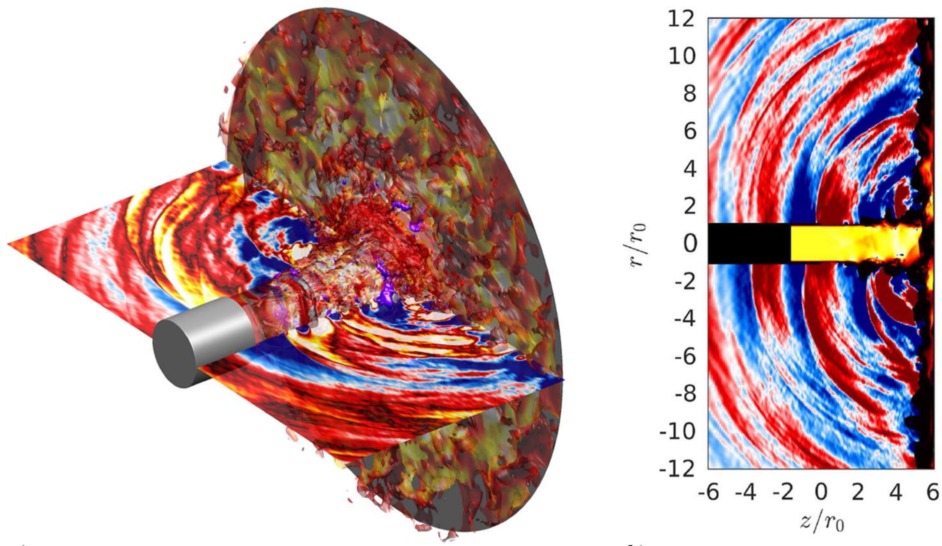

a) b)

Fig. 1 Representation for JetidealL6 of a) isosurfaces of 1.3 $\mathrm{kg \cdot m^{-3}}$, colored by the Mach number, and the pressure field in the plane $\theta = 0$; b) snapshot in the (z,r) plane of the density in the jets and close to the flat plate and of the pressure fluctuations. The color scale ranges from 1 to 2 $\mathrm{kg \cdot m^{-3}}$ for the density and from −5000 to 5000 Pa for the fluctuating pressure.

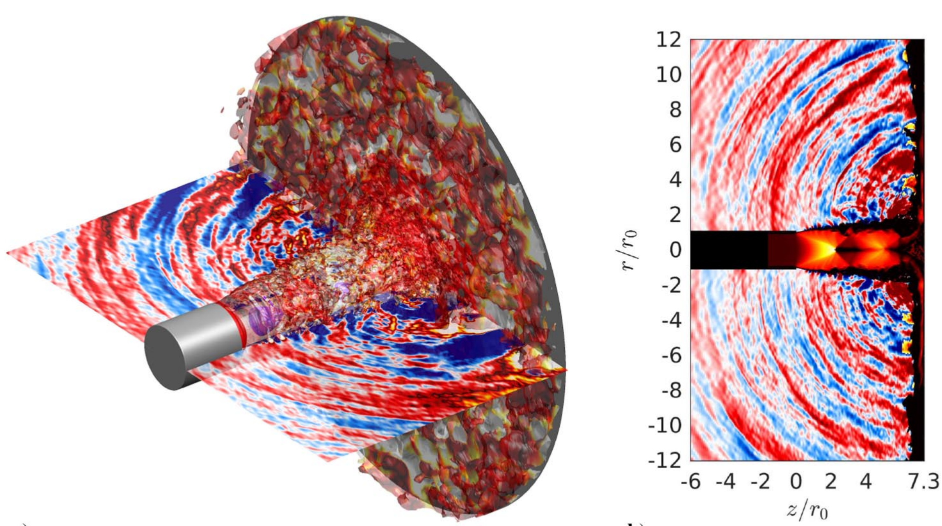

a) b)

Fig. 2 Representation for JetunderL7 of a) isosurfaces of density, the violet and red isosurfaces for the values of 0.95 and 2 $\mathrm{kg \cdot m^{-3}}$, respectively, isosurfaces of 1.25 $\mathrm{kg \cdot m^{-3}}$ colored by the Mach number, and the pressure field in the plane $\theta = 0$; b) snapshot in the (z,r) plane of the density in the jets and close to the flat plate and of the pressure fluctuations. The color scale ranges from 1 to 2 $\mathrm{kg \cdot m^{-3}}$ for the density and from −5000 to 5000 Pa for the fluctuating pressure.

direction. A complete description of the meshes can be found in the previous papers [16,17].

The discretization of the wall jet forming after the jet impact is analyzed at $r = 4r_0$. In the directions parallel to the wall, values of about $\Delta r^+ \simeq r\Delta\theta^+ \simeq 30$ are found for the four jets. Those values are similar to those used in the literature for the LES of turbulent boundary layers [28–30]. In the direction normal to the wall, values $\Delta z^+ \simeq 5$ are used. These values do not permit in theory to simulate with accuracy the turbulent boundary layer of the wall jet. However, using a similar solver, Bogey and Marsden [31] showed for the turbulent boundary layer developing in the nozzle of a turbulent subsonic jet that the LES results do not depend significantly on the mesh spacing in the direction normal to the wall for values $\Delta^+ = 3.7$ and below.

III. Feedback Loop

A. Snapshots

Three- and two-dimensional snapshots are represented in Figs. 1 and 2 for JetidealL6 and JetunderL7, respectively. For the three-dimensional (3-D) snapshots, to visualize both the flow and the acoustic fields of the jets, isosurfaces of density and pressure fields in the plane $\theta = 0$ are shown. For the two-dimensional (2-D) snapshots, the density is represented in the jet and near the wall, and the pressure field is displayed everywhere else.

The development of the jet shear layers are well visible and exhibit both large- and small-scale turbulent structures, in agreement with the Reynolds number of 6×10^4. In the pressure fields, acoustic waves coming from the region of jet impact and propagating in the upstream direction are noticed. In the 2-D snapshots, the density fields reveal the difference between JetidealL6, which is an ideally expanded jet with no shock-cell structure, and JetunderL7, which is an underexpanded jet with two shock cells visible. In the present study, the wall jets created after the jet impact, well visible on the 3-D snapshots, are studied.

B. Tone Frequencies

The pressure spectra obtained at $z = 0$ and $r = 2r_0$ for the two cases, for which snapshots are given in Sec. III.A (JetidealL6 and JetunderL7), are displayed in Fig. 3 as functions of the Strouhal

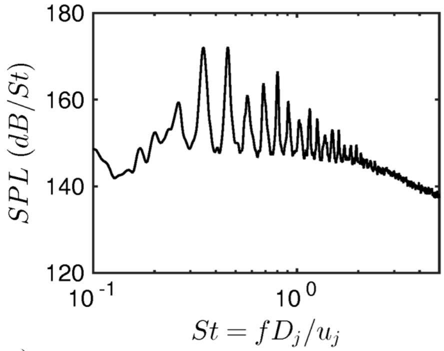

a)

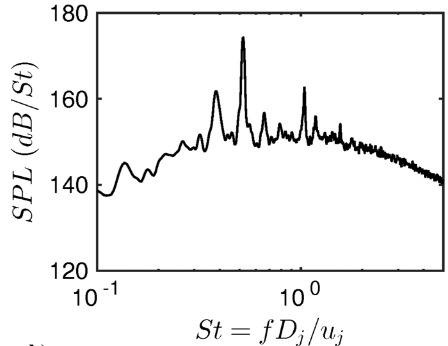

b)

Fig. 3 Sound pressure levels (SPLs) at $r = 2r_0$ and $z = 0$ as functions of the Strouhal number $St = fD_j/u_j$ for a) JetidealL6 and b) JetunderL7.

number $St = fD_j/u_j$. In Fig. 3a, about 10 tone frequencies are visible for JetidealL6, between $St = 0.2$ and $St = 2$, whereas only three can be seen for JetunderL7 in Fig. 3b.

For the other jets, the sound pressure levels obtained in the vicinity of the nozzle also reveal several tone frequencies [16,17]. The first four Strouhal numbers of the tones for which the levels are 5 dB higher than the broadband noise are reported in Table 2. The tones are generated by an aeroacoustic feedback mechanism occurring between the nozzle and the plate. A good agreement has been found between the tone frequencies of the present simulated jet, those found in the experimental studies of Henderson et al. [7] and Krothapalli et al. [6], and the frequencies predicted by the classical feedback model [3,4]. The corresponding comparisons are available in previous papers [16,17].

Overall, for the ideally expanded jets, about 10 tones are noticed, as observed for ideally expanded planar supersonic jets experimentally [32] and numerically [33]. On the contrary, only two or three dominant tones are found for the nonideally expanded jets, as already noted in various experimental studies [6,7,34,35].

For each of these tone frequencies, the corresponding axisymmetric or helical jet oscillation and the associated mode number in the classical model proposed by Ho and Nosseir [3] and Nosseir and Ho [4] have been identified [16,17]. The results are given in Table 3, and they will be used in the next sections.

IV. Flow Properties near the Flat Plate

This section deals with the flow properties in the wall jet region, where no experimental data are available. Comparisons of mean fields and turbulent levels with experimental data in the jets are available in previous papers [16,17].

A. Flowfield Statistics

The mean radial velocities obtained for the four ideally expanded jets are represented in Fig. 4, where z_w is the axial location of the plate. The wall jets are created at $r \sim r_0$, where the jet shear layers impinge on the plate. The peak radial velocities of the wall jets are equal to $0.913u_j$ for JetidealL6, $0.870u_j$ for JetidealL8, $0.847u_j$ for JetidealL10, and $0.820u_j$ for JetidealL12. As expected, the larger the nozzle-to-plate distance, the lower the maximum radial velocity in the wall jet.

The rms values of the radial velocity fluctuations are displayed in Fig. 5 for the four ideally expanded jets. The jet shear layers and the wall jets both appear clearly. Higher values are found in the wall jets than in the jet shear layers. The maximal values in the wall jets decrease with the nozzle-to-plate distance, yielding $0.232u_j$ for JetidealL6, $0.209u_j$ for JetidealL8, $0.193u_j$ for JetidealL10, and $0.180u_j$ for JetidealL12. The position where the maximal value is reached varies from $2.1r_0$ for JetidealL6 up to $4.0r_0$ for JetidealL12.

The mean radial velocity of the four nonideally expanded jets are shown in Fig. 6. The shock-cell structures of the jets are visible, leading to positive and negative values of the mean radial velocity. The presence of the shock-cell structure results in the formation of a recirculation bubble near the plate, at $r \sim r_0$, visible thanks to the isocontour for $\langle u_r \rangle = -0.05u_j$ in Fig. 6. Moreover, in this case, the variation of the maximal value of the mean radial velocity with the nozzle-to-plate distance is not monotonous, and they are equal to $0.897u_j$ for JetunderL4, $0.956u_j$ for JetunderL5, $0.963u_j$ for JetunderL7, and $0.893u_j$ for JetunderL9. Finally, using isocontours for $\langle u_r \rangle = 0.9u_j$, shock cells appear in the wall jet for JetunderL5 and JetunderL7, for which the highest mean radial velocities are found. For those two jets, the cylindrical wall jet is thus organized with annular shock-cell structures.

For the four underexpanded jets, the rms values of radial velocity fluctuations are represented in Fig. 7. For JetunderL4, JetunderL5, and JetunderL9, the Mach disk formed just upstream from the plate [16] is visible. Downstream from the Mach disk, a shear layer is created in the jet and spreads to the wall by expanding in the radial direction, creating a conical area of high turbulence intensity. This area represents the recirculation bubble with flow moving from the position where the jet shear layers impinge on the plate to the center of the Mach disk, about one radius upstream from the plate. In the wall jets, the maximal rms value of the radial velocity decreases with the nozzle-to-plate distance and is equal to $0.226u_j$ for JetunderL4, $0.195u_j$ for JetunderL5, $0.191u_j$ for JetunderL7, and $0.182u_j$ for JetunderL9.

Table 2 Strouhal numbers emerging in the pressure spectra in the vicinity of the nozzle[a]

	St_1	St_2	St_3	St_4
JetidealL6	0.26	0.345	**0.455**	0.57
JetidealL8	0.205	0.29	0.365	**0.445**
JetidealL10	0.165	0.29	0.375	**0.44**
JetidealL12	0.175	0.255	0.305	**0.38**
JetunderL4	0.375	**0.505**	1.01	——
JetunderL5	0.335	**0.415**	——	——
JetunderL7	**0.345**	0.42	——	——
JetunderL9	0.27	**0.34**	0.42	——

[a]Strouhal numbers of the dominant tones are in bold.

Table 3 Mode number and oscillation nature of the jet oscillations at the first four tone Strouhal numbers

	St_1	St_2	St_3	St_4
JetidealL6	$N = 2$, hel.	$N = 3$, hel.	$N = 4$, axi.	$N = 5$, hel.
JetidealL8	$N = 2$, axi.	$N = 3$, hel.	$N = 4$, axi.	$N = 5$, axi.
JetidealL10	$N = 2$, axi.	$N = 4$, hel.	$N = 5$, axi.	$N = 6$, axi.
JetidealL12	$N = 3$, axi.	$N = 4$, hel.	$N = 5$, hel.	$N = 6$, axi.
JetunderL4	$N = 2$, hel.	$N = 3$, axi.	——	——
JetunderL5	$N = 2$, hel.	$N = 3$, hel.	——	——
JetunderL7	$N = 3$, hel.	$N = 4$, hel.	——	——
JetunderL9	$N = 3$, hel.	$N = 4$, hel.	$N = 5$, hel.	——

The terms hel. or axi. denote helical and axisymmetric.

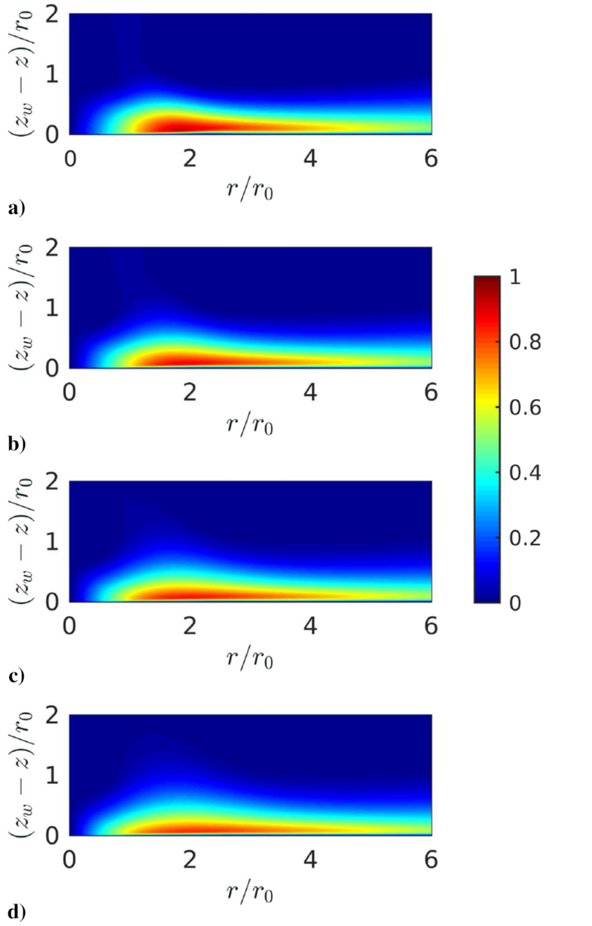

Fig. 4 Mean radial velocity $\langle u_r \rangle / u_j$ for a) JetidealL6, b) JetidealL8, c) JetidealL10, and d) JetidealL12.

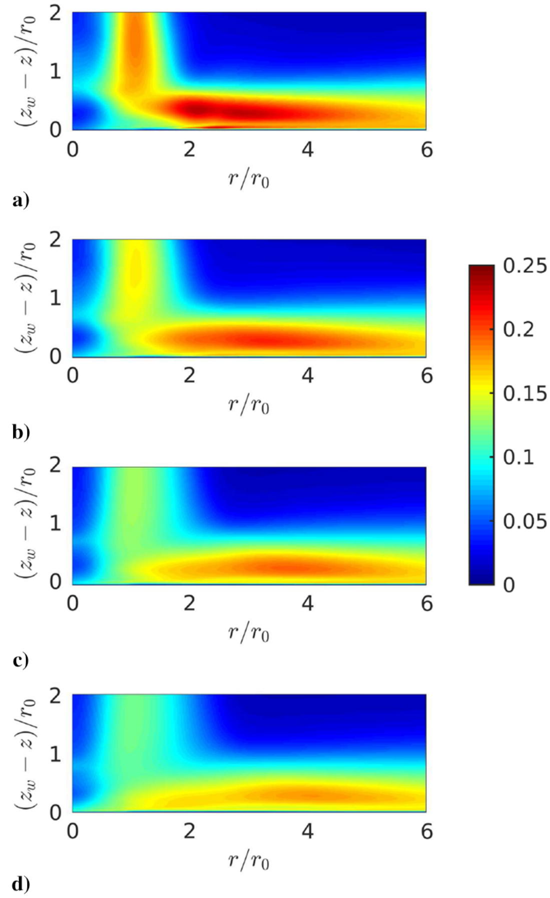

Fig. 5 Root mean square values of radial velocity fluctuations $u_{r,\mathrm{rms}}/u_j$ for a) JetidealL6, b) JetidealL8, c) JetidealL10, and d) JetidealL12.

Overall, for the ideally expanded jets, the maximal mean and rms values of the radial velocity in the wall jets decrease with the nozzle-to-plate distance, as expected. However, for the underexpanded jets, the presence of the shock-cell structure appears to affect the maximal mean velocity in the wall jet. Indeed, the highest value is found for JetunderL7, for which there is no Mach disk just upstream of the plate [16]. The presence of the oblique shock just upstream of the plate in JetunderL7 thus seems to enable the jet shear layer to deviate and become a wall jet, leading to high-velocity speeds close to the wall.

B. Pressure and Density Fields on the Plate

1. Snapshots

During the LES, pressure has been recorded in the planes $z=0$, $z = L$, and $\theta = 0$. Moreover, density has also been stored in the plane $z=L$. A Fourier decomposition of the fields is carried out, permitting one to plot the amplitude and phase fields for a given frequency.

Snapshots of the density and pressure fields obtained at the wall for the ideally expanded jets are presented in Fig. 8. A movie showing the temporal evolution of the fields is also available online. In the density fields, high values are found at the center of the domain, in the region of jet impact. Turbulent structures coming from the jet shear layers are observed to propagate radially in the movie. In the pressure fields, the exact location of the jet impact clearly appears. It is not perfectly round, nor centered. Turbulent structures propagating radially can be also be seen. The larger area of the jet impact in the density field than in the pressure fields is most likely because the jet is cold.

Density and pressure snapshots are represented in Fig. 9 for the four underexpanded jets, and a corresponding movie is given online. In the density field, low values of density are found around $r = 0$. This results from the presence of a shock-cell structure, seen in Fig. 2b. Turbulent structures from the jet shear layers impinge on the plate and travel radially. Similar observations can be made for the pressure fields. In particular, for JetunderL4, concentric rings are visible in Figs. 9a and 9e. The rings are due to the dominant axisymmetric mode of the aeroacoustic feedback mechanism identified for this jet in Gojon and Bogey [16]. Indeed, at the frequency of the dominant resonant frequency, axisymmetrically organized turbulent structures are noticed in the jet shear layers.

2. Pressure Spectra

The pressure spectra obtained for the four ideally expanded jets are represented in Fig. 10 as a function of the radial coordinate. The frequencies of the feedback mechanism all emerge between $r = 0$ and $r \approx 1.5r_0$, where the shear layers impinge on the plate, but only some of them remain visible for $r > 1.5r_0$, in the wall jet created after the impact. In the latter case, fewer tone frequencies appear for larger nozzle-to-plate distances.

To be more quantitative, the pressure spectra obtained at $r = 0$, $r = r_0$, and $r = 4r_0$ for the four ideally expanded jets are represented in Fig. 11. As expected, because of the shear layer impingement, higher broadband levels are observed at $r = r_0$ than at the two other locations. The tone frequencies all appear at $r = 0$ and $r = r_0$, but only some of them are visible at $r = 4r_0$, for JetidealL6 and JetidealL8.

The pressure spectra obtained in the plate for the underexpanded jets are displayed in Fig. 12 as a function of the radial coordinate. As previously, the frequencies of the feedback mechanism are all visible between $r = 0.5r_0$ and $r \approx 1.5r_0$, but only some of them emerge for $r > 1.5r_0$. However, one clear difference with respect to the ideally expanded jets is that, for most of the frequencies, the contribution seems negligible close to $r = 0$. Only one frequency, namely, the main frequency of JetunderL4 at $St_2 = 0.505$, clearly appears in this region. This frequency corresponds to the only frequency associated with a strong motion of the near-wall Mach disk [16].

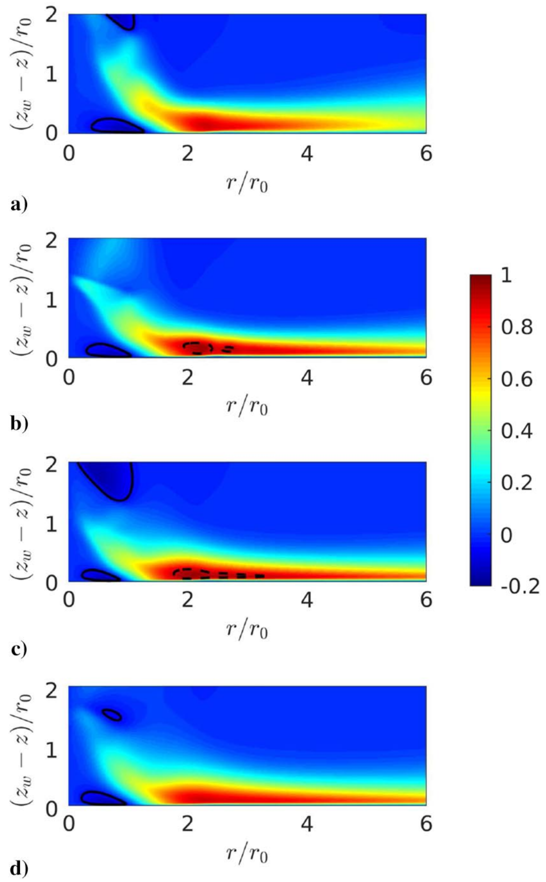

Fig. 6 Mean radial velocity $\langle u_r \rangle / u_j$ for a) JetunderL4, b) JetunderL5, c) JetunderL7, and d) JetunderL9 (solid and dashed lines indicate the isocontours for $\langle u_r \rangle = -0.05 u_j$ and $\langle u_r \rangle = 0.9 u_j$, respectively).

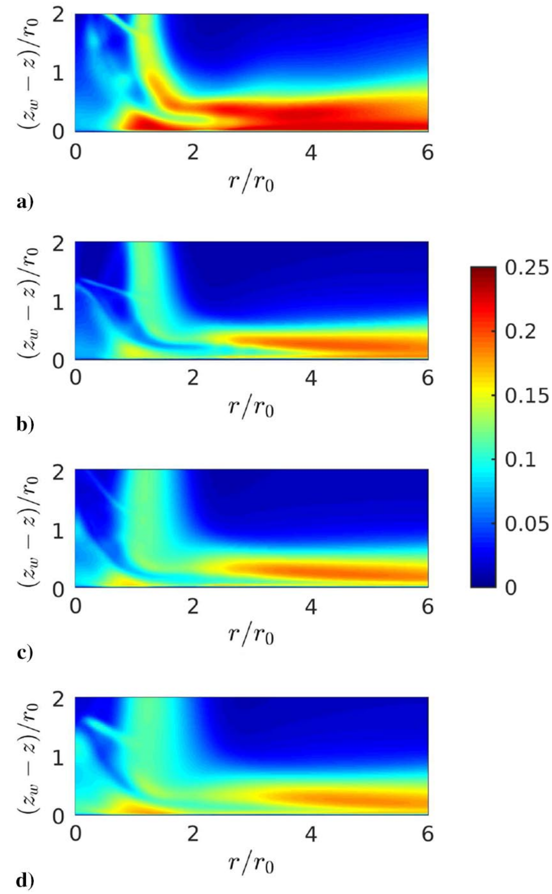

Fig. 7 Root mean square values of radial velocity fluctuations $u_{r,\mathrm{rms}}/u_j$ for a) JetunderL4, b) JetunderL5, c) JetunderL7, and d) JetunderL9.

The pressure spectra obtained at $r = 0$, $r = r_0$, and $r = 4r_0$ for the underexpanded jets are presented in Fig. 13. Similar to the results for the ideally expanded jets, strong broadband components are found at $r = r_0$. All the feedback tone frequencies also emerge at this location. However, compared with the ideally expanded jets for which all the tone frequencies can be seen on the jet axis, only the dominant tone frequency of JetunderL4 at $St_2 = 0.505$ and its harmonics are visible at $r = 0$.

3. *Fourier Decomposition*

The amplitude and phase fields obtained for JetunderL4 at the two main tone frequencies at $St_1 = 0.375$ and $St_2 = 0.505$ are now presented in Figs. 14 and 15, respectively.

The amplitude and phase fields of the fluctuating pressure obtained at $z = 0$ for $St_1 = 0.375$ are given in Figs. 14a and 14e. The amplitude field does not exhibit a clear pattern. On the contrary, the phase field shows two opposite regions out of phase on both sides of the jet axis, followed by isophase contours of spiral shape. This indicates a helical organization of the acoustic waves. In the plane $\theta = 0$, in the phase field of Fig. 14f, a 180 deg phase shift is visible with respect to the jet axis, suggesting a sinuous or helical oscillation mode of the jet. More precisely, from a Fourier decomposition of the fluctuating pressure in the azimuthal direction at $z = 0$ and $r = 2r_0$, the mode is helical. The amplitude and phase fields of the fluctuating pressure obtained on the plate are reported in Figs. 14c and 14g. The amplitude field reveals a region of high intensity for $r < 2.6r_0$ in the jet flow region. Looking at the amplitude field represented in Fig. 14b, this area is located downstream from the Mach disk and the annular oblique shock. The phase field, in Fig. 14g, shows a spiral that extends over the entire domain. The amplitude and phase fields of the fluctuating density on the plate are presented in Figs. 14d and 14h. They exhibit the same properties as those of the pressure fluctuations. The turbulent structures organized helically in the jet shear layers at the tone frequency $St_1 = 0.375$ impinge on the plate, and they seem to keep the same organization as they propagate radially on the plate.

The amplitude and phase fields of the fluctuating pressure and density determined for JetunderL4 at $St_2 = 0.505$ are represented in Fig. 15. The results obtained at $z = 0$ for the pressure are given in Figs. 15a and 15e. The acoustic waves appear to be organized in an axisymmetric manner. The amplitude field in the plane $\theta = 0$ of Fig. 15b reveals a cell structure between the nozzle and the plate, containing three cells. This structure is due to the generation of a hydrodynamic-acoustic standing wave by the aeroacoustic feedback mechanism. The number of cells in the standing wave is equal to the mode number of the feedback mechanism in the model of Ho and Nosseir [3], as shown by Gojon et al. [33] using a model of an hydrodynamic-acoustic standing wave proposed by Panda et al. [36]. The phase field at $\theta = 0$, in Fig. 15f, exhibits a symmetric organization with respect to the jet axis, corresponding to an axisymmetric oscillation mode. In Figs. 15g and 15h, concentric rings are observed in the phase fields of the fluctuating pressure and of the fluctuating density on the plate. These rings are probably due to the radial propagation, on the plate, of the coherent structures organized axisymmetrically in the jet shear layers.

To confirm the preceding claims, phase profiles are plotted in Fig. 16. The profile in Fig. 16a is that obtained in the $\theta = 0$ plane, along the black line visible in the phase field of Fig. 15f. It is represented in Fig. 16a as a function of the distance l_{impact} from the point on the wall at $z = 3r_0$. This point is chosen because it corresponds approximately to the location of the source of the acoustic component radiating in the far field, see in Henderson et al. [7] and in Gojon and Bogey [16], The maxima in the phase profile are located at $l_{\mathrm{impact}} = r_0$, $4.25r_0$, and $7.6r_0$, giving wavelengths of $3.25r_0$ and $3.35r_0$, hence phase speeds of $327\ \mathrm{m \cdot s^{-1}}$ and $338\ \mathrm{m \cdot s^{-1}}$, respectively. These velocities are close to the ambient sound speed, as expected for acoustic waves. In Fig. 16b, the phase profile obtained in the $z = L$ plane along the black line shown in Fig. 15g is depicted as

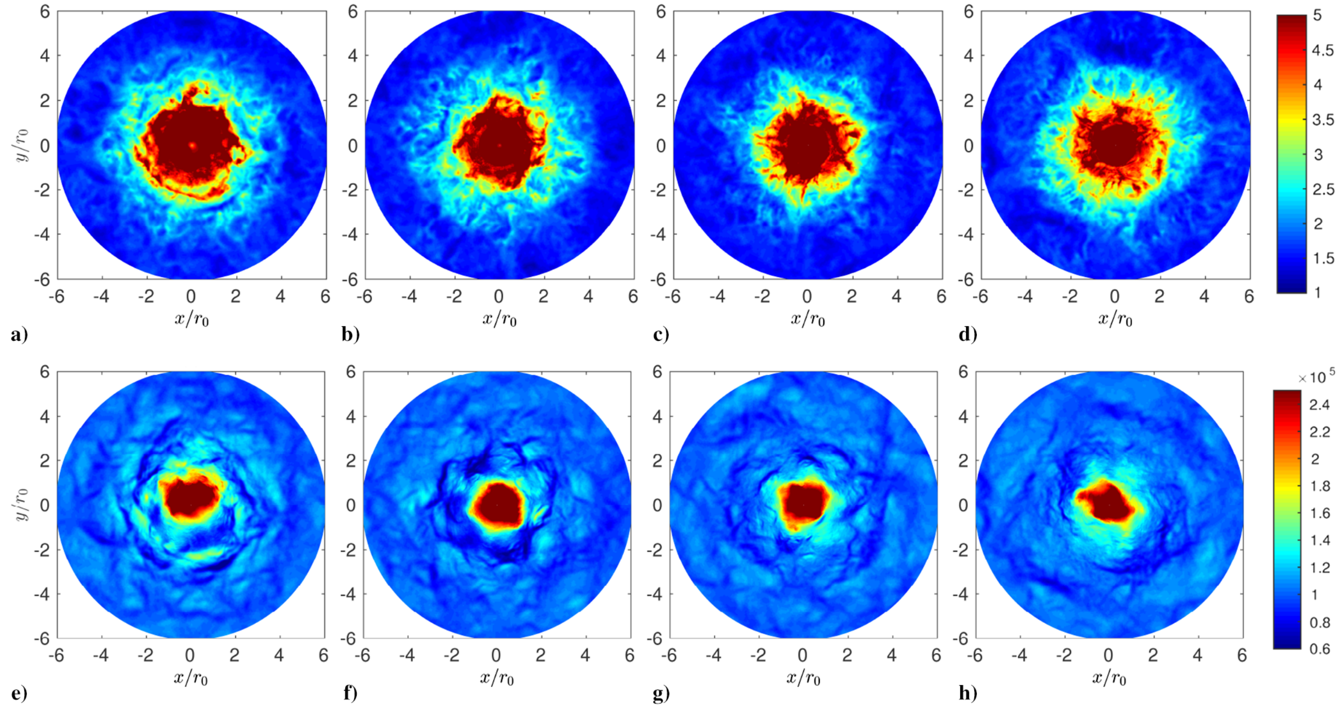

Fig. 8 Density (top) and pressure (bottom) fields on the plate obtained for a,e) JetidealL6; b,f) JetidealL8; c,g) JetidealL10; and d,h) JetidealL12. The color scales range from 1 to 5 $\mathrm{kg \cdot m^{-3}}$ for density and from 60,000 to 250,000 Pa for pressure.

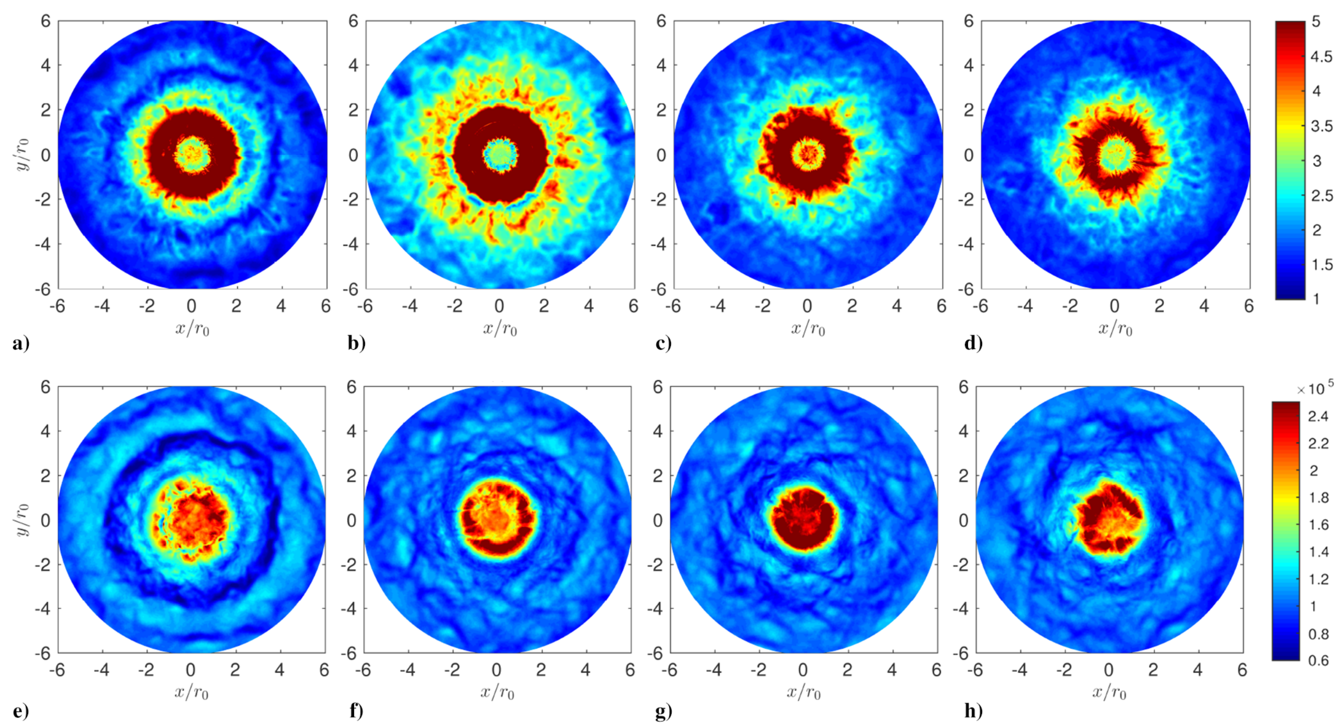

Fig. 9 Density (top) and pressure (bottom) fields on the plate obtained for a,e) JetunderL4; b,f) JetunderL5; c,g) JetunderL7; and d,h) JetunderL9. The color scales range from 1 to 5 $\mathrm{kg \cdot m^{-3}}$ for density and from 60,000 to 250,000 Pa for the pressure.

a function of the radial coordinate. The wavelengths of the concentric rings apparent in Figs. 15g and 15h can thus be measured. They are equal to $1.75r_0$ between the first and the second maxima and to $2.15r_0$ between the second and the third maxima, yielding phase speeds of $0.40u_j$ and $0.49u_j$, respectively. Therefore, the pressure and density patterns obtained at the wall cannot be due to acoustic waves, but are associated with the radial convection of turbulent structures in the wall jets. Thus, for the nonideally expanded jets, the temporal organization of the wall jet along the frequencies of the feedback mechanism seems to be linked to the oscillations of the Mach disk located just upstream of the plate. Indeed, for JetunderL4, the Mach disk located just upstream of the plate strongly oscillates at $St_2 = 0.505$ [16]. A movie given in a previous paper [16] allows us to see the Mach disk pumping and forcing the turbulent structure to stay organized from the jet shear layers to the wall jet. Finally, it is interesting to note that the two tone frequencies of JetunderL4 are produced simultaneously [16]; the axisymmetrical and the spiral organizations of the wall jet are thus establishing at the same time.

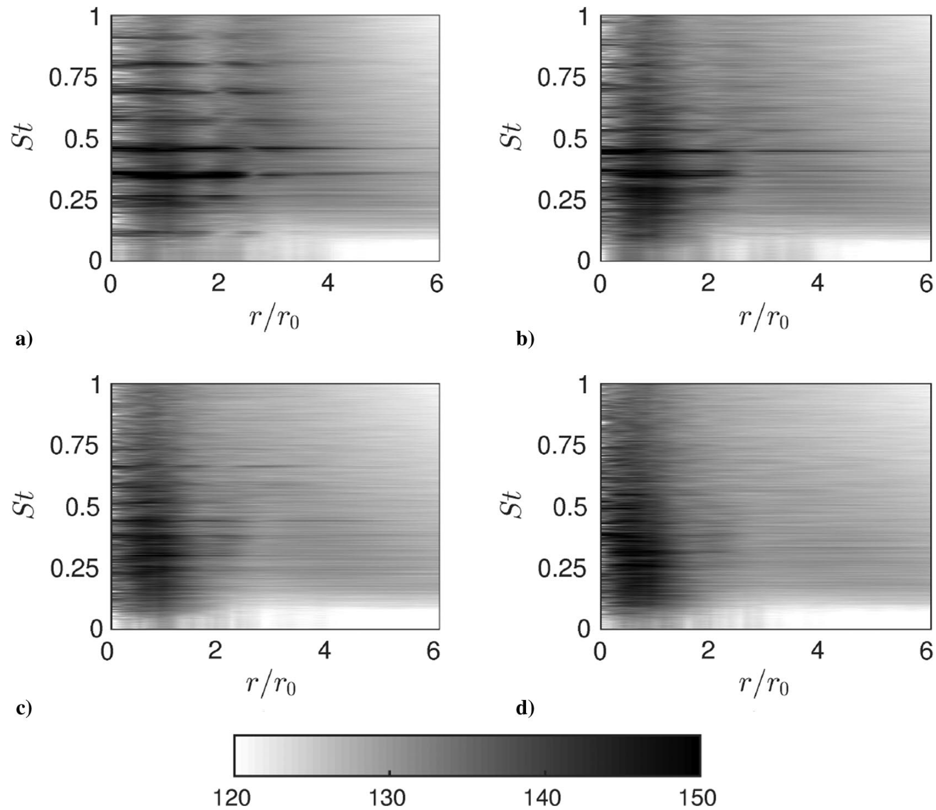

Fig. 10 Pressure spectra obtained on the plate as functions of radial coordinate and Strouhal number for a) JetidealL6, b) JetidealL8, c) JetidealL10, and d) JetidealL12. The color scale ranges from 120 to 150 dB/St.

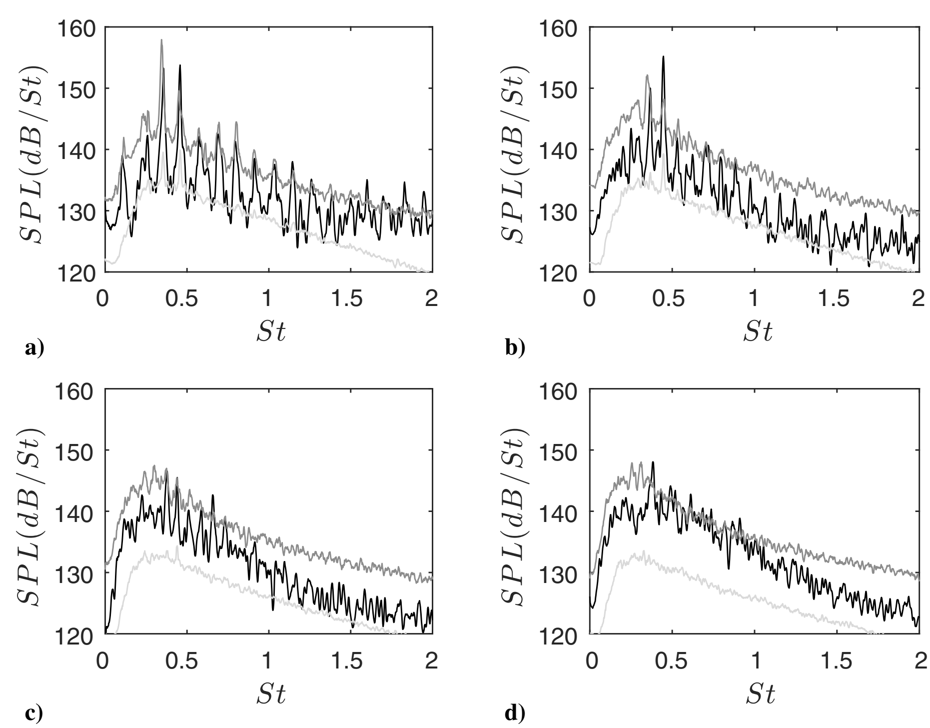

Fig. 11 Pressure spectra obtained on the plate at $r = 0$ (black line), $r = r_0$ (dark grey line), and $r = 4r_0$ (light grey line), as a function of Strouhal number for a) JetidealL6, b) JetidealL8, c) JetidealL10, and d) JetidealL12.

For the ideally expanded jet JetidealL6, the results obtained at the main tone frequency at $St_3 = 0.455$ are represented in Fig. 17. The amplitude field at $\theta = 0$ of Fig. 17b reveals a cell structure between the nozzle and the plate, containing four cells. This structure is due to the generation of a hydrodynamic-acoustic standing wave by the aeroacoustic feedback mechanism, and the number of cells is equal to the mode number of the feedback mechanism [33]. Moreover, a symmetric organization with respect to the jet axis appears in the phase field of Fig. 17f. The jet thus undergoes an axisymmetric oscillation at $St_3 = 0.455$. In Figs. 17g and 17h, concentric rings are observed in the

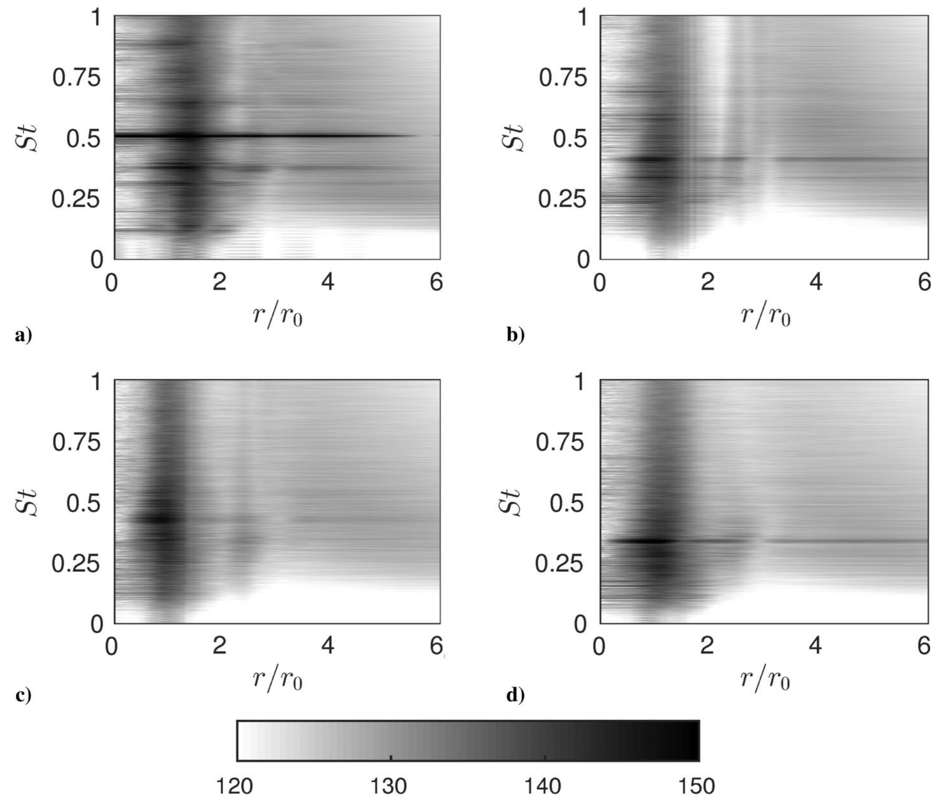

Fig. 12 Pressure spectra obtained on the plate as functions of radial coordinate and Strouhal number for a) JetunderL4, b) JetunderL5, c) JetunderL7, and d) JetunderL9. The color scale ranges from 120 to 150 dB/St.

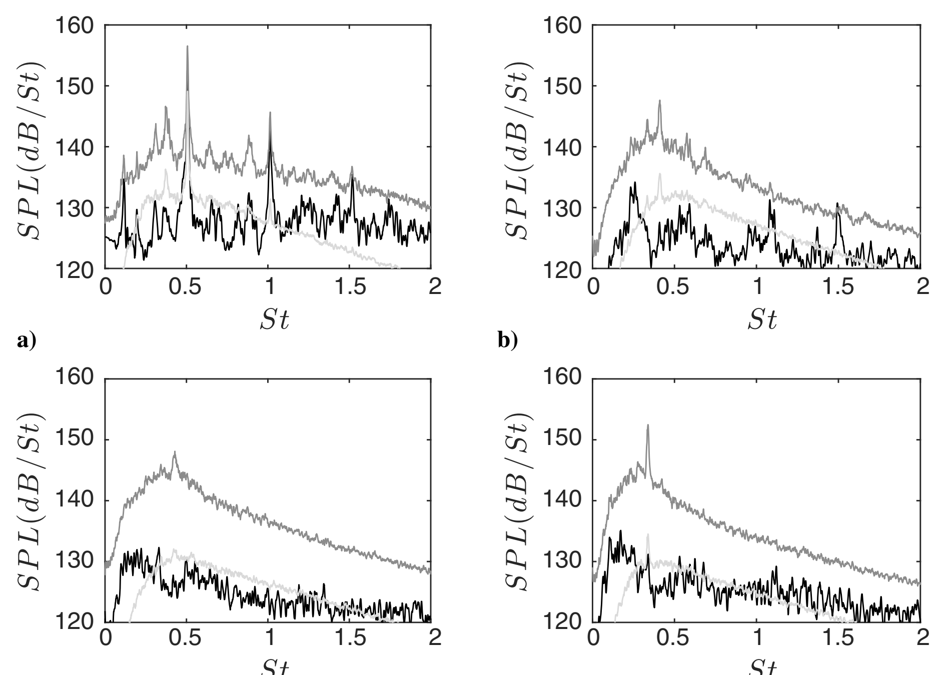

Fig. 13 Pressure spectra obtained on the plate at $r = 0$ (black line), $r = r_0$ (dark grey line), and $r = 4r_0$ (light grey line), as a function of Strouhal number for a) JetunderL4, b) JetunderL5, c) JetunderL7, and d) JetunderL9.

phase fields of the fluctuating pressure and density on the plate. These rings result from the radial propagation, on the plate, of the coherent structures organized axisymmetrically in the jet shear layers.

4. *Convection Velocity of Turbulent Structures in Wall Jets*

To give further insight into the convection velocity of the structures in the wall jets in all cases, the pressure phase fields on the plate are investigated in the same way as for JetunderL4 in Fig. 16b. First, let us consider two regions of interest. The first one is near the jet axis over $0 < r < 3r_0$, and the second one is several diameters away over $3r_0 < r < 6r_0$. The mean wavelengths are extracted from the phase profiles in each of the two regions and the corresponding convection velocities are given in Table 4.

Over $3r_0 < r < 6r_0$, the convection velocity of the turbulent structures on the wall varies between $0.40u_j$ and $0.49u_j$, and no clear

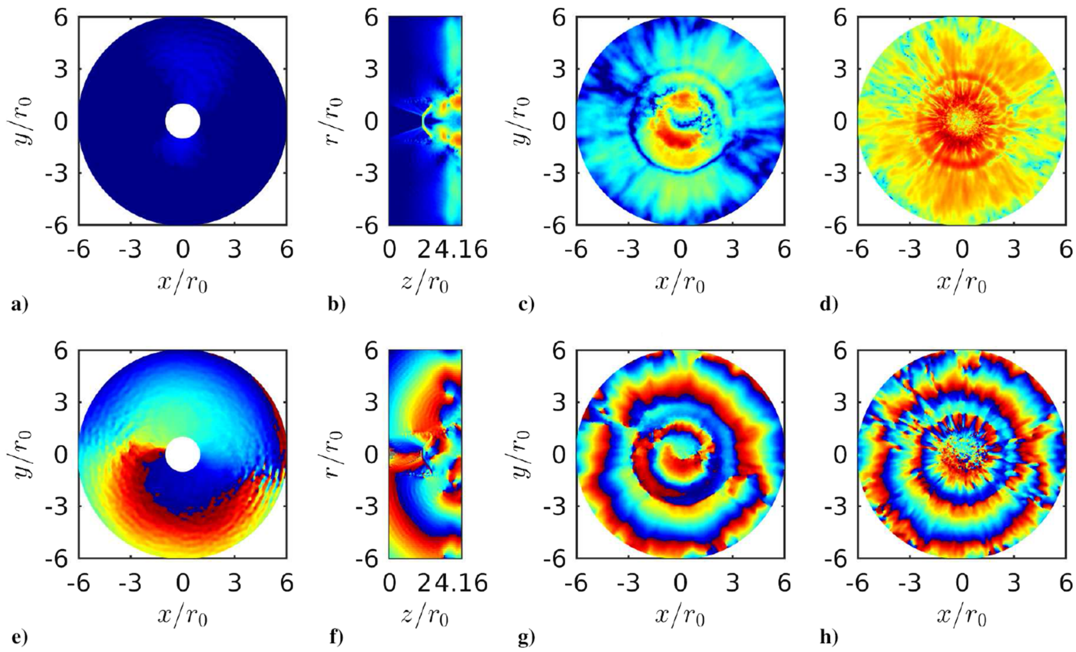

Fig. 14 Amplitude (top) and phase (bottom) fields obtained for JetunderL4 at the tone frequency $St_1 = 0.375$: from pressure a,e) at $z = 0$; b,f) at $\theta = 0$; and c,g) at $z = L$; and from density d,h) at $z = L$. The color scales range from 120 to 160 dB/St for the amplitude fields of pressure, from zero to one for the normalized amplitude field of density, and from $-\pi$ to π for the phase fields.

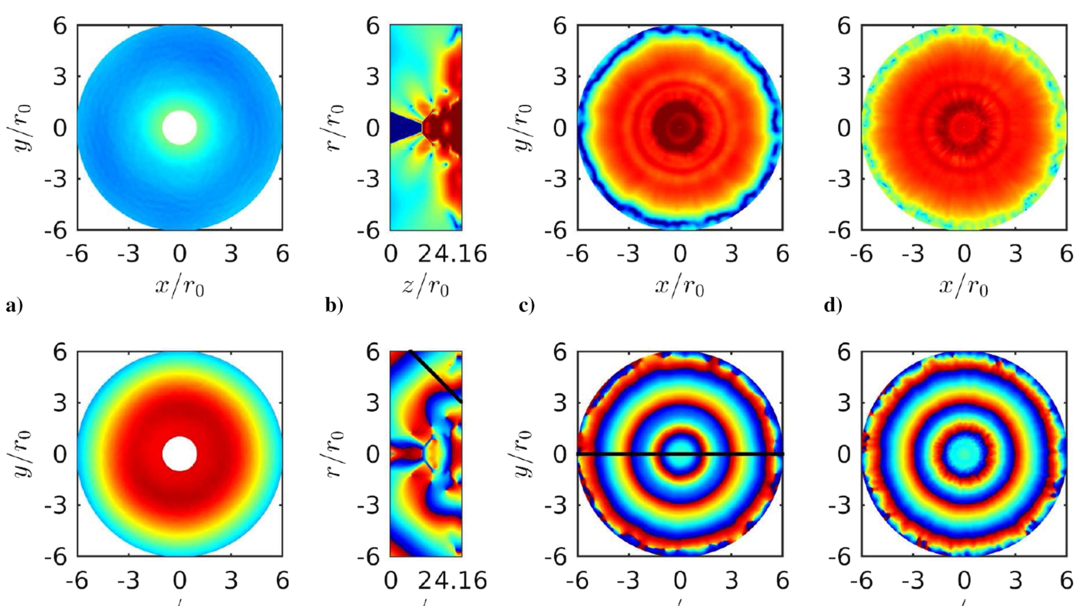

Fig. 15 Amplitude (top) and phase (bottom) fields obtained for JetunderL4 at the dominant tone frequency $St_2 = 0.505$: from pressure a,e) at $z = 0$; b,f) at $\theta = 0$; and c,g) at $z = L$; and from density d,h) at $z = L$. The color scales range from 120 to 160 dB/St for the amplitude fields of pressure, from zero to one for the normalized amplitude field of density, and from $-\pi$ to π for the phase fields.

distinctions can be made between the ideally expanded jets and the underexpanded ones. The results are in agreement with the measurements of Davis et al. [15] for ideally expanded impinging round jets, who found a convection velocity on the wall equal to $0.47u_j$ several diameters away from the jet axis by using pressure-sensitive paint on the flat plate. The results are also consistent with the mean convection velocity of the turbulent structures in the jet shear layers, which is between $0.54u_j$ and $0.59u_j$ for the four underexpanded jets [16].

Over $0 < r < 3r_0$, the convection velocity of the turbulent structures on the wall varies between $0.27u_j$ and $0.57u_j$. These values are in agreement with the value of $0.56u_j$ found experimentally by Davis et al. [15] in this region for ideally expanded impinging round jets. The convection velocities are between $0.45u_j$ and $0.57u_j$ for the ideally expanded jets, but between $0.27u_j$ and $0.40u_j$ for the nonideally expanded jets. This difference is likely caused by the presence of a Mach disk in the near-wall region for the nonideally expanded jets, as observed in Fig. 6. The jet shear layers are thus deviated and impinge on the plate at $r \simeq 2r_0$. Consequently, the mean convection velocities computed near the jet axis do not correspond to the convection velocity of the turbulent structures, because the motion of these structures is not only radial in this region. On the contrary, in the ideally expanded jets, the turbulent structures in the jet shear layers impinge near the jet axis, as illustrated by Krothapalli et al. [6] and Davis et al. [15] and observed in Fig. 4. Finally, it is interesting to note that, for JetunderL4, in the region $3r_0 < r < 6r_0$, the convection velocity of the structures organized axisymmetrically at the tone frequency $St_2 = 0.505$ is 22.5% higher than the

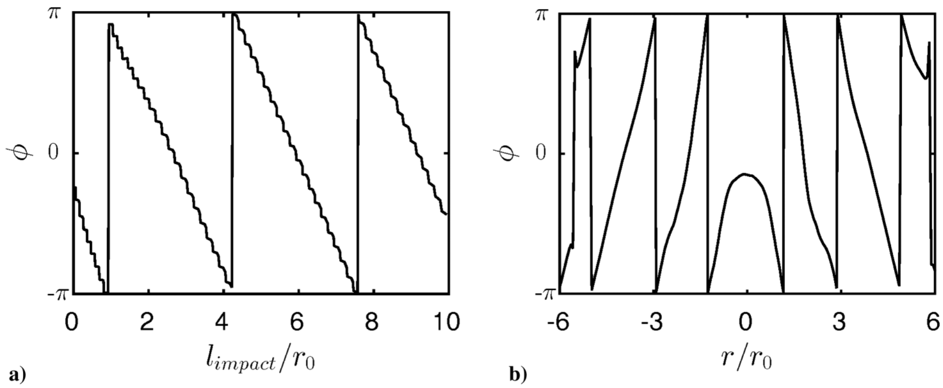

Fig. 16 Phase profiles obtained for JetunderL4 at $St_2 = 0.505$: a) in the plane $\theta = 0$ along the black line represented in Fig. 15f; and b) at $z = L$ along the black line in Fig. 15g.

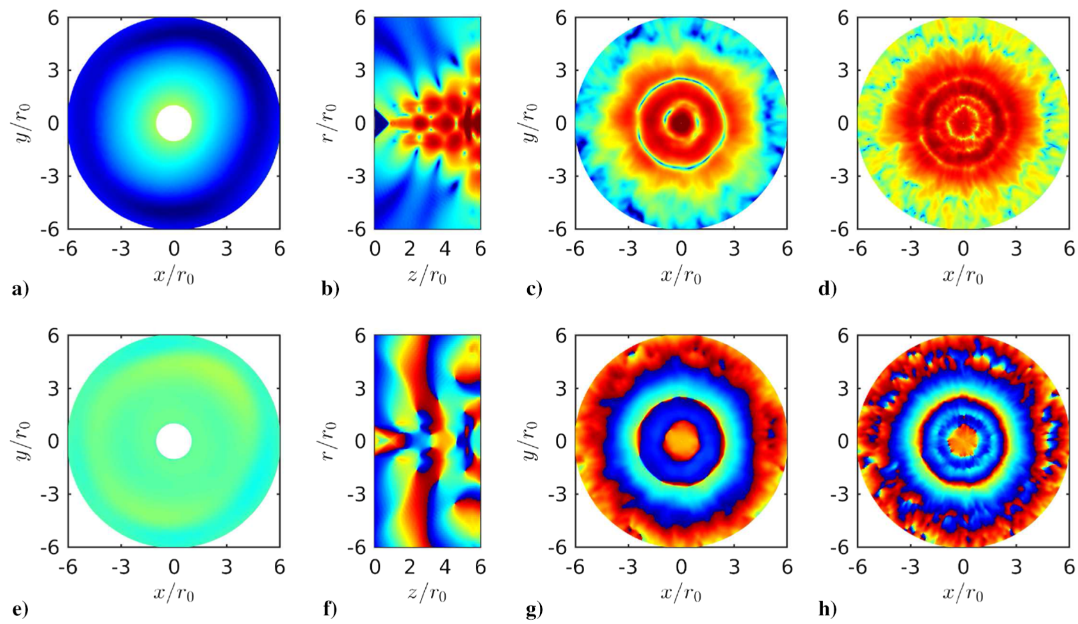

Fig. 17 Amplitude (top) and phase (bottom) fields obtained for JetidealL6 at the tone frequency $St_3 = 0.455$: from pressure a,e) at $z = 0$; b,f) at $\theta = 0$, and c,g) at $z = L$; and from density d,h) at $z = L$. The color scales range from 120 to 160 dB/St for the amplitude fields of pressure, from zero to one for the normalized amplitude field of density, and from $-\pi$ to π for the phase fields.

convection velocity of the turbulent structures organized helically at $St_1 = 0.375$.

The convection velocity in the wall jets is now computed from radial velocity cross correlations just upstream from the wall, at a fixed wall-normal position of $0.1r_0$. This position has been chosen for two reasons. First, it is difficult to follow the position of maximum rms velocity, because it is usually done to compute the convection velocity of the turbulent structures in the shear layers [37,38] in free jets, because of the complex flow patterns that arise near the jet axis, notably for the nonideally expanded jets (see Fig. 7). Then, to compare the results with those obtained experimentally using pressure-sensitive paint and those of the present paper from pressure phase fields on the plate, the convection velocity needs to be computed very close to the wall. The results are represented in Fig. 18a for the ideally expanded jets and in Fig. 19a for the nonideally expanded jets as a function of the radial position between $r = 0$ and $r = 6r_0$. The maximal mean radial velocity in the wall jets is also provided in Figs. 18b and 19b. This velocity correspond to the signed velocity, where the absolute value of the radial velocity is maximal in the wall jet, permitting also a look at the recirculation region. For the ideally expanded jets, in Fig. 18a, the convection velocity increases from zero to about $0.55u_j$ from $r = 0$ to $r = 2.5r_0$. It then decreases slowly in the region $r \geq 2.5r_0$ to reach $0.38r_0$ at $r = 6r_0$. These results are in good agreement with the convection velocities obtained from the phase profiles in Table 4 and with those measured in the phase-averaged distributions of the fluctuating pressure of the ideally expanded jets of Davis et al. [15].

Table 4 Mean convection velocities of the turbulent structures in the wall jets for different main tone frequencies

Jet	St	$u_c(0 < r < 3r_0)$	$u_c(3r_0 < r < 6r_0)$
JetidealL6	$St_2 = 0.345$	$u_c = 0.57u_j$	$u_c = 0.49u_j$
JetidealL6	$St_3 = 0.455$	$u_c = 0.54u_j$	$u_c = 0.47u_j$
JetidealL8	$St_4 = 0.445$	$u_c = 0.51u_j$	$u_c = 0.45u_j$
JetidealL10	$St_4 = 0.44$	$u_c = 0.49u_j$	$u_c = 0.43u_j$
JetidealL12	$St_4 = 0.38$	$u_c = 0.45u_j$	$u_c = 0.41u_j$
JetunderL4	$St_1 = 0.375$	$u_c = 0.27u_j$	$u_c = 0.40u_j$
JetunderL4	$St_2 = 0.505$	$u_c = 0.40u_j$	$u_c = 0.49u_j$
JetunderL5	$St_2 = 0.415$	$u_c = 0.35u_j$	$u_c = 0.47u_j$
JetunderL7	$St_2 = 0.345$	$u_c = 0.38u_j$	$u_c = 0.48u_j$
JetunderL9	$St_2 = 0.34$	$u_c = 0.34u_j$	$u_c = 0.46u_j$

For the nonideally expanded jets, in Fig. 19a, a region of negative convection velocity appears around $r = r_0$ for JetunderL4, JetunderL5, and JetunderL7. This is due to the presence of a recirculation bubble near the region of impact, observed experimentally for similar jets by Krothapalli et al. [6]. This recirculation zone leads in Fig. 19b to a negative mean radial velocity for $r < r_0$. It explains the difference between the convection velocities previously noticed over $0 < r < 3r_0$ for the underexpanded and the ideally expanded jets. A peak convection

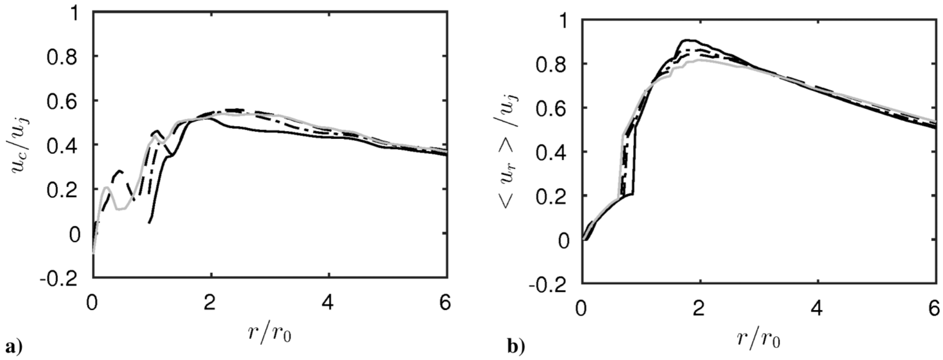

Fig. 18 Variation with the radial distance of a) the convection velocity computed from the cross correlations of radial velocity fluctuations just upstream from the wall and b) the maximal mean radial velocity in the wall jet for JetidealL6 (solid line), JetidealL8 (dash-dot line), JetidealL10 (dashed line), and JetidealL12 (grey line).

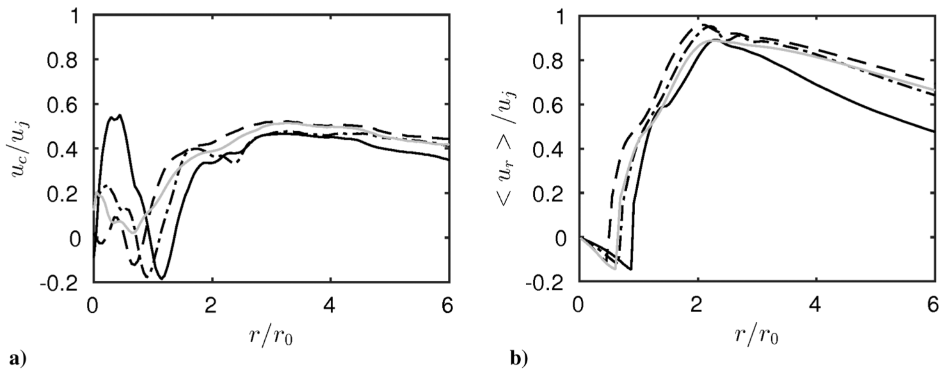

Fig. 19 Variation with the radial distance of a) the convection velocity computed from the cross correlations of radial velocity fluctuations just upstream from the wall and b) the maximal radial velocity in the wall jet for JetunderL4 (solid line), JetunderL5 (dash-dot line), JetunderL7 (dashed line), and JetunderL9 (grey line).

velocity between $0.45u_j$ and $0.5u_j$ is then reached at $r \sim 3r_0$ before a slow decrease in the region $r \geq 3r_0$ to reach values between $0.44u_j$ and $0.69u_j$ at $r = 6r_0$.

The maximal radial velocity in the wall jet is higher in the nonideally expanded jets than in the ideally expanded ones, but the opposite trend is noted for the convection velocity.

V. Conclusions

In this paper, the flow properties near the flat plate for ideally expanded and nonideally expanded impinging round jets have been studied using compressible large-eddy simulation. They have been characterized in the jet shear layers, and also on the flat plate, to examine the wall jets created after the jet impact. For all jets, the spectra in the near pressure fields revealed several tone frequencies due to a feedback mechanism occurring between the nozzle lips and the flat plate. The near pressure and density fields of the jets are then analyzed using fast Fourier transform on the nozzle exit plane, the plate plane, and an azimuthal plane. It is found that the helical or axisymmetric organization of the turbulent structures in the jet shear layers, specific to each tone frequency, persists after the jet impact on the plate. The radial propagation of these structures in the wall jets leads to a spiral or to concentric rings in the phase fields, respectively. In particular, for one of the jets, a spiral shape and concentric rings are observed at two different tone frequencies. Finally, the convection velocity of the turbulent structures in the wall jets is evaluated from the phase fields and cross correlations of radial velocity. Over $3r_0 < r < 6r_0$, the convection velocity of the structures varies between $0.40u_j$ and $0.49u_j$ in the present jets. These results are in agreement with measurements for supersonic impinging round jets performed using pressure-sensitive paint on the flat plate. Near the jet axis, differences are observed between the ideally expanded jets and the nonideally expanded ones, with negative convection velocities found around the lip-line radial position in the latter case. Finally, for the nonideally expanded jets, the temporal organization of the wall jet along the frequencies of the feedback mechanism seems to be linked to the oscillation of the Mach disk located just upstream of the plate, pumping and forcing the turbulent structure to stay organized from the jet shear layers to the wall jet.

Acknowledgments

The simulations presented in the paper were performed using the high-performance-computing resources of Fédération Lyonnaise de Modélisation et Sciences Numériques, partner of Equipex Equip@meso and of Centre Informatique National de l'Enseignement Supérieur, under the allocation 2016-2a0204 made by Grand Equipement National de Calcul Intensif. This work was performed within the framework of the Labex CeLyA of Université de Lyon, within the program "Investissements d'Avenir" (ANR-10-LABX-0060/ANR-11-IDEX-0007) operated by the French National Research Agency.

References

[1] Powell, A., "On Edge Tones and Associated Phenomena," *Acta Acustica United with Acustica*, Vol. 3, No. 4, 1953, pp. 233–243.
[2] Wagner, F., "The Sound and Flow Field of an Axially Symmetric Free Jet Upon Impact on a Wall," NASA TT F-13942, 1971.
[3] Ho, C., and Nosseir, N., "Dynamics of an Impinging Jet. Part 1. The Feedback Phenomenon," *Journal of Fluid Mechanics*, Vol. 105, April 1981, pp. 119–142.
doi:10.1017/S0022112081003133
[4] Nosseir, N., and Ho, C., "Dynamics of an Impinging Jet. Part 2. The Noise Generation," *Journal of Fluid Mechanics*, Vol. 116, March 1982, pp. 379–391.
doi:10.1017/S0022112082000512
[5] Henderson, B., and Powell, A., "Experiments Concerning Tones Produced by an Axisymmetric Choked Jet Impinging on Flat Plates," *Journal of Sound and Vibrations*, Vol. 168, No. 2, 1993, pp. 307–326.
doi:10.1006/jsvi.1993.1375
[6] Krothapalli, A., Rajkuperan, E., Alvi, F., and Lourenco, L., "Flow Field and Noise Characteristics of a Supersonic Impinging Jet," *Journal of*

Fluid Mechanics, Vol. 392, 1999, pp. 155–181.
doi:10.1017/S0022112099005406

[7] Henderson, B., Bridges, J., and Wernet, M., "An Experimental Study of the Oscillatory Flow Structure of Tone-Producing Supersonic Impinging Jets," *Journal of Fluid Mechanics*, Vol. 542, Nov. 2005, pp. 115–137.
doi:10.1017/S0022112005006385

[8] Risborg, A., and Soria, J., "High-Speed Optical Measurements of an Underexpanded Supersonic Jet Impinging on an Inclined Plate," *28th International Congress on High-Speed Imaging and Photonics*, Vol. 7126F, 2009, pp. 1–11.
doi:10.1117/12.822137

[9] Buchmann, N., Mitchell, D., Ingvorsen, K., Honnery, D., and Soria, J., "High Spatial Resolution Imaging of a Supersonic Underexpanded Jet Impinging on a Flat Plate," *Sixth Australian Conference on Laser Diagnostics in Fluid Mechanics and Combustion*, 2011, pp. 1–4.

[10] Mitchell, D., Honnery, D., and Soria, J., "The Visualization of the Acoustic Feedback Loop in Impinging Underexpanded Supersonic Jet Flows Using Ultra-High Frame Rate Schlieren," *Journal of Visualization*, Vol. 15, No. 4, 2012, pp. 333–341.
doi:10.1007/s12650-012-0139-9

[11] Kuo, C., and Dowling, A., "Oscillations of a Moderately Underexpanded Choked Jet Impinging upon a Flat Plate," *Journal of Fluid Mechanics*, Vol. 315, May 1996, pp. 267–291.
doi:10.1017/S002211209600242X

[12] Dauptain, A., Cuenot, B., and Gicquel, L., "Large Eddy Simulation of Stable Supersonic Jet Impinging on Flat Plate," *AIAA Journal*, Vol. 48, No. 10, 2010, pp. 2325–2338.
doi:10.2514/1.J050362

[13] Dauptain, A., Gicquel, L., and Moreau, S., "Large Eddy Simulation of Supersonic Impinging Jets," *AIAA Journal*, Vol. 50, No. 7, 2012, pp. 1560–1574.
doi:10.2514/1.J051470

[14] Weightman, J., Amili, O., Honnery, D., Soria, J., and Edgington-Mitchell, D., "An Explanation for the Phase Lag in Supersonic Jet Impingement," *Journal of Fluid Mechanics*, Vol. 815, 2017, pp. 1–11.
doi:10.1017/jfm.2017.37

[15] Davis, T., Edstrand, A., Alvi, F., Cattafesta, L., Yorita, D., and Asai, K., "Investigation of Impinging Jet Resonant Modes Using Unsteady Pressure-Sensitive Paint Measurements," *Experiments in Fluids*, Vol. 56, No. 5, 2015, pp. 1–0.
doi:10.1007/s00348-015-1976-9

[16] Gojon, R., and Bogey, C., "Flow Structure Oscillations and Tone Production in Underexpanded Impinging Round Jets," *AIAA Journal*, Vol. 55, No. 6, 2017, pp. 1792–1805.
doi:10.2514/1.J055618

[17] Bogey, C., and Gojon, R., "Feedback Loop and Upwind-Propagating Waves in Ideally-Expanded Supersonic Impinging Round Jets," *Journal of Fluid Mechanics*, Vol. 823, 2017, pp. 562–591.
doi:10.1017/jfm.2017.334

[18] Bogey, C., and Bailly, C., "A Family of Low Dispersive and Low Dissipative Explicit Schemes for Flow and Noise Computations," *Journal of Computational Physics*, Vol. 194, No. 1, 2004, pp. 194–214.
doi:10.1016/j.jcp.2003.09.003

[19] Berland, J., Bogey, C., Marsden, O., and Bailly, C., "High-Order, Low Dispersive and Low Dissipative Explicit Schemes for Multiple-Scale and Boundary Problems," *Journal of Computational Physics*, Vol. 224, No. 2, 2007, pp. 637–662.
doi:10.1016/j.jcp.2006.10.017

[20] Bogey, C., and Bailly, C., "Large Eddy Simulations of Transitional Round Jets: Influence of the Reynolds Number on Flow Development and Energy Dissipation," *Physics of Fluids*, Vol. 18, No. 6, 2006, Paper 065101.
doi:10.1063/1.2204060

[21] Bogey, C., and Bailly, C., "Turbulence and Energy Budget in a Self-Preserving Round Jet: Direct Evaluation Using Large Eddy Simulation," *Journal of Fluid Mechanics*, Vol. 627, 2009, pp. 129–160.
doi:10.1017/S0022112009005801

[22] Fauconnier, D., Bogey, C., and Dick, E., "On the Performance of Relaxation Filtering for Large-Eddy Simulation," *Journal of Turbulence*, Vol. 14, No. 1, 2013, pp. 22–49.
doi:10.1080/14685248.2012.740567

[23] Tam, C., and Dong, Z., "Wall Boundary Conditions for High-Order Finite-Difference Schemes in Computational Aeroacoustics," *Theoretical and Computational Fluid Dynamics*, Vol. 6, Nos. 5–6, 1994, pp. 303–322.
doi:10.1007/BF00311843

[24] Bogey, C., de Cacqueray, N., and Bailly, C., "A Shock-Capturing Methodology Based on Adaptative Spatial Filtering for High-Order Non-Linear Computations," *Journal of Computational Physics*, Vol. 228, No. 5, 2009, pp. 1447–1465.
doi:10.1016/j.jcp.2008.10.042

[25] Mohseni, K., and Colonius, T., "Numerical Treatment of Polar Coordinate Singularities," *Journal of Computational Physics*, Vol. 157, No. 2, 2000, pp. 787–795.
doi:10.1006/jcph.1999.6382

[26] Bogey, C., de Cacqueray, N., and Bailly, C., "Finite Differences for Coarse Azimuthal Discretization and for Reduction of Effective Resolution near Origin of Cylindrical Flow Equations," *Journal of Computational Physics*, Vol. 230, No. 4, 2011, pp. 1134–1146.
doi:10.1016/j.jcp.2010.10.031

[27] Bogey, C., Marsden, O., and Bailly, C., "Large-Eddy Simulation of the Flow and Acoustic Fields of a Reynolds Number 10^5 Subsonic Jet with Tripped Exit Boundary Layers," *Physics of Fluids*, Vol. 23, No. 3, 2011, Paper 035104.
doi:10.1063/1.3555634

[28] Viazzo, S., Dejoan, A., and Schiestel, R., "Spectral Features of the Wall-Pressure Fluctuations in Turbulent Wall Flows with and Without Perturbations Using LES," *International Journal of Heat and Fluid Flow*, Vol. 22, No. 1, 2001, pp. 39–52.
doi:10.1016/S0142-727X(00)00074-6

[29] Gloerfelt, X., and Berland, J., "Direct Computation of Turbulent Boundary Layer Noise," AIAA Paper 2009-3401, 2009, pp. 1–22.
doi:10.2514/6.2009-3401

[30] Schlatter, P., Li, Q., Brethouwer, G., Johansson, A., and Henningson, D., "Simulations of Spatially Evolving Turbulent Boundary Layers up to $Re_\theta = 4300$," *International Journal of Heat and Fluid Flow*, Vol. 31, No. 3, 2010, pp. 251–261.
doi:10.1016/j.ijheatfluidflow.2009.12.011

[31] Bogey, C., and Marsden, O., "Simulations of Initially Highly Disturbed Jets with Experiment-Like Exit Boundary Layers," *AIAA Journal*, Vol. 54, No. 4, 2016, pp. 1299–1312.
doi:10.2514/1.J054426

[32] Norum, T., "Supersonic Rectangular Jet Impingement Noise Experiments," *AIAA Journal*, Vol. 29, No. 7, 1991, pp. 1051–1057.
doi:10.2514/3.10703

[33] Gojon, R., Bogey, C., and Marsden, O., "Investigation of Tone Generation in Ideally Expanded Supersonic Planar Impinging Jets Using Large-Eddy Simulation," *Journal of Fluid Mechanics*, Vol. 808, 2016, pp. 90–115.
doi:10.1017/jfm.2016.628

[34] Powell, A., "The Sound-Producing Oscillations of Round Underexpanded Jets Impinging on Normal Plates," *Journal of the Acoustical Society of America*, Vol. 83, No. 2, 1988, pp. 515–533.
doi:10.1121/1.396146

[35] Henderson, B., "The Connection Between Sound Production and Jet Structure of the Supersonic Impinging Jet," *Journal of the Acoustical Society of America*, Vol. 111, No. 2, 2002, pp. 735–747.
doi:10.1121/1.1436069

[36] Panda, J., Raman, G., and Zaman, K., "Underexpanded Screeching Jets from Circular, Rectangular and Elliptic Nozzles," AIAA Paper 1997-1623, 1997.
doi:10.2514/6.1997-1623

[37] André, B., "Etude Expérimentale de L'effet du vol sur le Bruit de choc de Jets Supersoniques Sous-Détendus," Ph.D. Thesis, Ecole Centrale de Lyon, Écully, France, 2012.

[38] Gojon, R., and Bogey, C., "Simulations of Initially Highly Disturbed Jets with Experiment-Like Exit Boundary Layers," *International Journal of Aeroacoustics* (to be published).

P. G. Tucker
Associate Editor